

# Advantages of statistical analysis of giant vesicle flickering for bending elasticity measurements

P. Méléard<sup>1,a</sup>, T. Pott<sup>1</sup>, H. Bouvrais<sup>1,2</sup>, and J.H. Ipsen<sup>2</sup>

<sup>1</sup> Université Européenne de Bretagne, UMR CNRS-ENSCR 6226 “Sciences Chimiques de Rennes”, ENSCR, Avenue du Général Leclerc, CS 50837, F-35708 Rennes Cedex 7, France

<sup>2</sup> Department of Physics and Chemistry, MEMPHYS - Center for Biomembrane Physics, University of Southern Denmark, Campusvej 55, DK-5230 Odense M, Denmark

Received 28 June 2011

Published online: 27 October 2011 – © EDP Sciences / Società Italiana di Fisica / Springer-Verlag 2011

**Abstract.** We show how to greatly improve precision when determining bending elasticity of giant unilamellar vesicles. Taking advantage of the well-known quasi-spherical model of liposome flickering, we analyze the full probability distributions of the configurational fluctuations instead of limiting the analysis to the second moment measurements only as usually done in previously published works. This leads to objective criteria to reject vesicles that do not behave according to the model. As a result, the confidence in the bending elasticity determination of individual vesicles that fit the model is improved and, consequently, the reproducibility of this measurement for a given membrane system. This approach uncovers new possibilities for bending elasticity studies like detection of minute influences by solutes in the buffer or into the membrane. In the same way, we are now able to detect the inhomogeneous behavior of giant vesicle systems such as the hazardous production of peroxide in bilayers containing fluorescent dyes.

## 1 Introduction

Giant unilamellar vesicles, GUVs, have been intensively used for the last 30 years by physics and biophysics. As model membranes with a controlled composition, they were employed to investigate behaviors known to be important for biological activity like mechanical properties [1–5] and raft hypothesis [6–9]. Quite generally, these studies involved one-component lipid bilayers, lipid mixtures, lipid and protein mixtures and rarely, membrane extracts [6,10–15]. GUVs made of simple lipid bilayers were also involved when investigating the effects of non-absorbing chemicals [16,17] or additional components partitioning between the buffer and the vesicle bilayer (for example, see [18]). The reasons why GUVs became one of the most popular vesicle systems are twofold. First, their huge size allows direct observation using optical microscopy, and second, GUV production methods are nowadays easy to reproduce [16,17,19–22].

The ability of membrane systems to bend under very low stress is perhaps the most obvious mechanical property of such soft materials. This softness is characterized by bending elasticity,  $k_c$ , whose measurement is intrinsically difficult due to its very small value (from a few  $k_B T$  to about  $100k_B T$  depending on the bilayer composition). Following the introduction of the role of bending elasticity

in membrane systems by Helfrich in 1973 [23], its very first estimation was made in 1975 on red blood cell membranes, using the flickering phenomenon originating from thermal fluctuations [24]. From then on, different approaches involving bilayer model systems of defined composition have led to various methods to estimate bending elasticity. The first category is based on the observation of freely moving vesicles submitted to thermal fluctuations using either tubular [1,25,26] or quasi-spherical vesicles [2,4,14,27–35]. The second category measures the response of the membrane to mechanical deformation originating from micropipette aspiration techniques [3,5,36–38], tether formation [39–41], bead diffusion [42], optical force in a confocal microscope [43–45] or electric field [46]. The last category involves peak shape analysis of X-ray diffraction by multilamellar systems [47].

About 20 years ago, we developed a method based on the observation and the measurement of thermal fluctuations of GUVs seen by phase-contrast video-microscopy and evaluated by digitized image analysis. Simply, we were computing the autocorrelation function of the GUV contour fluctuations and worked on the amplitudes obtained after Legendre polynomials decomposition [4]. At that time, we had to take into account important technical limits. The video signal was analog and the total number of digitized images was small ( $\approx 400$ ). Also, the measured amplitudes had to be corrected for the video integration time [4]. Finally, analysis was restricted to a small

<sup>a</sup> e-mail: philippe.meleard@ensc-rennes.fr

number of GUVs for a given system, due to the inefficient GUV production method based on spontaneous swelling (adapted from [48]).

Nowadays, the bending elasticity of a given GUV is obtained from a much larger number of digitized images (several 2000 images over 1 min series [33]; 3000 to 4000 images over 2 to 3 min [18]; about 15000 images over 10 min [49]) which improves the accuracy of the measurement. Other technical refinements were also made, like an optical system [50] or a simpler stroboscopic illumination set-up [51], to limit the exposure time of the video camera. Ultimately, GUV can now be produced quite efficiently using different methods recently published in the literature [16, 17, 19–22].

Despite these numerous improvements, a weak point persists in the measurement of  $k_c$  from fluctuating quasi-spherical GUVs. Whatever the precise details of the methods, it always starts with a selection of GUVs that should be considered for analysis. Ideally, the GUV should indeed be quasi-spherical, exhibiting measurable thermal fluctuations and without any attachment in order to agree with the theory used for the analysis. Yet, these criteria are not that clearly defined. It is the user who decides whether a GUV is too floppy or too tense for analysis. Likewise, the question remains whether a GUV can be reasonably considered as quasi-spherical and useful for analysis or as ellipsoidal and therefore excluded for  $k_c$  measurement. Further, only the GUV contour is observed, meaning that possible attachments elsewhere may be overlooked. Moreover, there might be cases of tiny defects associated to vesicle bilayer that cannot be detected using classical optical microscopy. A given vesicle may also be bilamellar rather than unilamellar, the image quality being usually not sufficient to distinguish easily between these two cases. To overcome all these difficulties, it is usually necessary to analyze typically 10 to 30 GUVs of a given system under chosen environment and to take the average  $k_c$  as the bending elasticity of the system [18]. It should be stressed that  $k_c$  values of individual GUVs may be quite scattered around such a mean value, especially if the user is not very rigorous in his selection process. In such cases the  $k_c$  value of an individual GUV poorly reflects the bending elasticity of the system, meaning that one has to increase dramatically the number of GUVs to track down subtle effects on membrane mechanical properties, such as small variations in membrane composition or solute concentration. A further difficulty arises from the fact that any method that obtains precision by measuring  $k_c$  as an average over several GUVs does not allow the detection of individual variations in the bending elasticity. For instance, small variations in composition of GUVs from the same batch may lead to scattered individual  $k_c$  values that cannot be distinguished from variations due to poor selection criteria.

Herein we present in details an improved method for measuring  $k_c$  from thermal fluctuations of GUVs. The main point of this improvement lies in the data analysis, that allows to judge GUV behaviors by their coherence with the theoretical description of thermal fluctuations of quasi-spherical vesicles. This results in a rigorous vesicle selection based on objective criteria making user bias negligible. Notably, the analysis reinforces the confidence

in the determination of bending elasticity of individual GUVs. This has already been proven in the context of photo-induced lipid peroxidation [49]. Therein we showed that GUVs from the same batch gave different  $k_c$  values, ranging from about  $1.2 \times 10^{-19}$  J to about  $2 \times 10^{-19}$  J related to the amount of lipid peroxidation that depends on the intensity and duration of the light exposure of each individual GUV.

In the following, we present the statistical description used for analyzing GUV fluctuations, followed by a detailed picture of experimentally observed thermal fluctuations of quasi-spherical vesicles. Based on the statistical behavior of GUVs, we present criteria that can be used to eliminate GUVs that do not fulfill the requirements for being treated according to the theory (quasi-spherical, absence of defects, etc.). Comparison with the earlier method highlights the advantages of the new one: all individual  $k_c$  values are close to the average bending elasticity, which itself is measured with largely increased precision. We conclude with a short presentation of the usefulness of the new method to detect true  $k_c$  variations in a given pool of GUVs, such as those caused by photo-induced lipid peroxidation [49].

## 2 Materials and methods

1-palmitoyl-2-oleoyl-*sn*-glycero-3-phosphocholine (POPC) and 1,2-dilauroyl-*sn*-glycero-3-phosphocholine (DLPC) were purchased from Avanti Polar Lipids Inc. (Birmingham, AL). 6-dodecanoyl-2-dimethylaminonaphthalene (LAURDAN), Texas Red 1,2-dipalmitoyl-*sn*-glycero-3-phosphoethanolamine, triethylammonium salt (TR-DPPE), 2-(6-(7-nitrobenz-2-oxa-1,3-diazol-4-yl) amino) hexanoyl-1-hexadecanoyl-*sn*-glycero-3-phosphocholine (NBD C6-HPC named NBD-PC in this work), lissamine rhodamine B 1,2-dihexadecanoyl-*sn*-glycero-3-phosphoethanolamine, triethylammonium salt (Rh-DPPE), 1,1'-dioctadecyl-3,3,3',3'-tetramethylindocarbocyanine perchlorate (DiIC18(3) named DiIC18 in this work) and 2-(4,4-difluoro-5,7-dimethyl-4-bora-3a,4a-diaza-s-indacene-3-pentanoyl)-1-hexadecanoyl-*sn*-glycero-3-phosphocholine ( $\beta$ -BODIPY FL C5-HPC named Bodipy-PC in this work) were obtained from Invitrogen, Denmark or France. Fluorophore stock concentrations were quantified by absorption spectroscopy using published absorption coefficients.

Giant unilamellar vesicles (GUVs) were prepared according to an already published protocol [16,17] using electroformation method. Briefly, a LUV suspension in water is prepared using a grinder mill (Retsch, Inc., Newton, PA) with a final lipid concentration of about 0.2 mg/mL. 5 deposits of 2  $\mu$ L are made on each electrode [17]. After water evaporation, the electroformation cell is filled with water or a buffer solution at 1 mmol/L Tris (Trizma Base, Sigma-Aldrich Chimie, France) and 1 mmol/L EDTA (ethylenediaminetetraacetic acid, Sigma-Aldrich Chimie, France) adjusted to pH 7.4. Next, an electrical field is applied using “low salinity” conditions as defined in [16,17].

At the end of the electroformation protocol, GUVs are detached from the electrodes and observed as freely moving objects under an Axiovert 135 microscope equipped

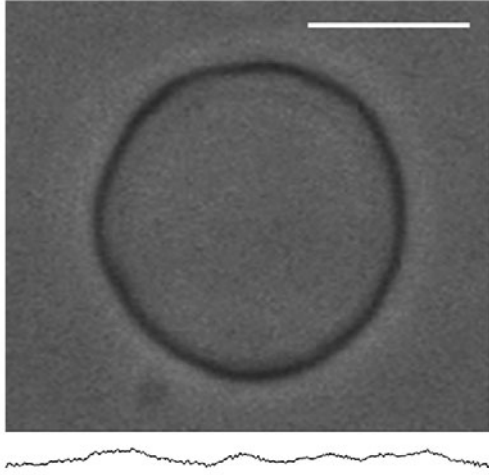


**Fig. 1.** Phase-contrast image of a giant vesicle after background subtraction. The bar at the top corresponds to  $10\ \mu\text{m}$ . At the bottom, the contour found after the extraction procedure is fluctuating around the mean radius (vertical axis), as a function of the angle  $\varphi$  (horizontal axis).

with a  $\times 63/0.75$  phase contrast objective (Zeiss, Germany). If necessary, the temperature inside the GUV chamber can be monitored. Stroboscopic illumination by a xenon flash lamp (flash FWHM =  $2.9\ \mu\text{s}$ , L7684 and its power supply, Hamamatsu, Japan) was used when studying GUV thermal fluctuations [50–52]. Video images were produced by a CCD C2400-77 (Hamamatsu, Japan) or a CCD DXC C33P (Sony, Japan) video-camera and recorded on a DSR-20P DVCAM recorder (Sony, Japan) for about 10 min.

The video image sequence of the GUV thermal fluctuations is analyzed on Apple<sup>TM</sup> laptop computers using a home-made software bundle developed under the MacOS X Leopard environment. Extraction of the vesicle contours is straightforward due to good contrast produced by phase-contrast microscopy after background subtraction, fig. 1. First, background images are obtained in a region free of GUVs using the settings of the optical microscope and video-camera chosen for GUV recording. We typically record 10 seconds of this region and make an average image of the corresponding 250 images. The obtained background image is smooth with intensity variation from place to place associated to optical defects in the optical path. During the following step of image analysis, this background is subtracted from every image of the contour fluctuations. This procedure leads to the images shown in fig. 2. The intensity variation as a function of the pixel position along a radius anchored at the contour center at a given angle  $\varphi$  is measured and the membrane position is obtained by fitting the intensity profile with a Lorentzian function. The number of images analyzed is typically 15000 (10 minutes at the European video frequency of 25 Hz) and the obtained contour radii,  $\rho(\varphi, t)$  ( $t$  is the time associated with the image), are then used for bending elasticity determination as detailed in the following. With fixed video-camera settings, the image illu-

mination is reproducible from one recording to the other because the flash lamp brilliance does not decrease measurably for weeks. This allows possible intensity comparison of the contour contrast obtained from different GUV recordings.

No correction was applied to the fluctuation measurements because of the stroboscopic illumination (FWHM =  $2.9\ \mu\text{s}$ ) that produces instantaneous snapshots of the vesicle deformations, removing any blurring effect associated with the video integration time [50–52]. This can be proved by comparing typical relaxation times  $\tau_m$  as estimated by Milner and Safran's theory [53] ( $\tau_m \sim 4\eta R^3 / (k_c m^3)$  for large enough fluctuation mode  $m$ , where  $\eta$  is the solvent viscosity and  $R$  the vesicle radius) with this FWHM. Choosing  $m = 40$ ,  $\eta = 10^{-3}\ \text{Pa}\cdot\text{s}$ ,  $R = 10\ \mu\text{m}$  and  $k_c = 1.2 \times 10^{-19}\ \text{J}$ , one finds  $\tau_{40}/\text{FWHM} > 150$ .

### 3 Statistical description of GUV flickering

The commonly used model for understanding thermal fluctuations of GUVs is to consider quasi-spherical vesicles, *i.e.*, vesicles whose fluctuations are not strong enough to lose the apparent mean spherical shape [4, 53]. Using notations already introduced in [4], one gets consequently

$$r(\theta, \varphi, t) = R[1 + u_0(\theta, \varphi) + \delta u(\theta, \varphi, t)], \quad (1)$$

where  $\theta$  and  $\varphi$  are the spherical angles,  $u_0$  and  $\delta u$  being the static mean shape and the time-dependent deformation of the vesicle. Using spherical harmonics  $Y_n^m$  as base functions [54], one obtains

$$r(\theta, \varphi, t) = R \left[ 1 + (A_0^0 + U_0^0(t))Y_0^0 + \sum_{n \geq 2, |m| \leq n}^{n_{\max}} U_n^m(t)Y_n^m(\theta, \varphi) \right], \quad (2)$$

where the only contribution to  $u_0$  is a constant term,  $A_0^0 Y_0^0$ , when considering quasi-spherical shapes [4]. Defining the time-dependent real functions  $a_n^m(t)$  and  $b_n^m(t)$  by  $U_n^m(t) = (a_n^m(t) - i b_n^m(t))/2$  with  $i = \sqrt{-1}$ , one can write eq. (2) as

$$r(\theta, \varphi, t) = R \left( 1 + (A_0^0 + U_0^0(t)) Y_0^0 + \left[ \sum_{n \geq 2}^{n_{\max}} a_n^0(t) \mathcal{P}_n^m(\cos \theta) + \sum_{0 < m \leq n} (a_n^m(t) \cos(m\varphi) + b_n^m(t) \sin(m\varphi)) \mathcal{P}_n^m(\cos \theta) \right] \right), \quad (3)$$

with  $\mathcal{P}_n^m(\cos \theta)$  related to the associated Legendre function  $P_n^m(\cos \theta)$  [54]

$$\mathcal{P}_n^m(\cos \theta) = (-1)^m \sqrt{\frac{2n+1}{4\pi} \frac{(n-m)!}{(n+m)!}} P_n^m(\cos \theta),$$

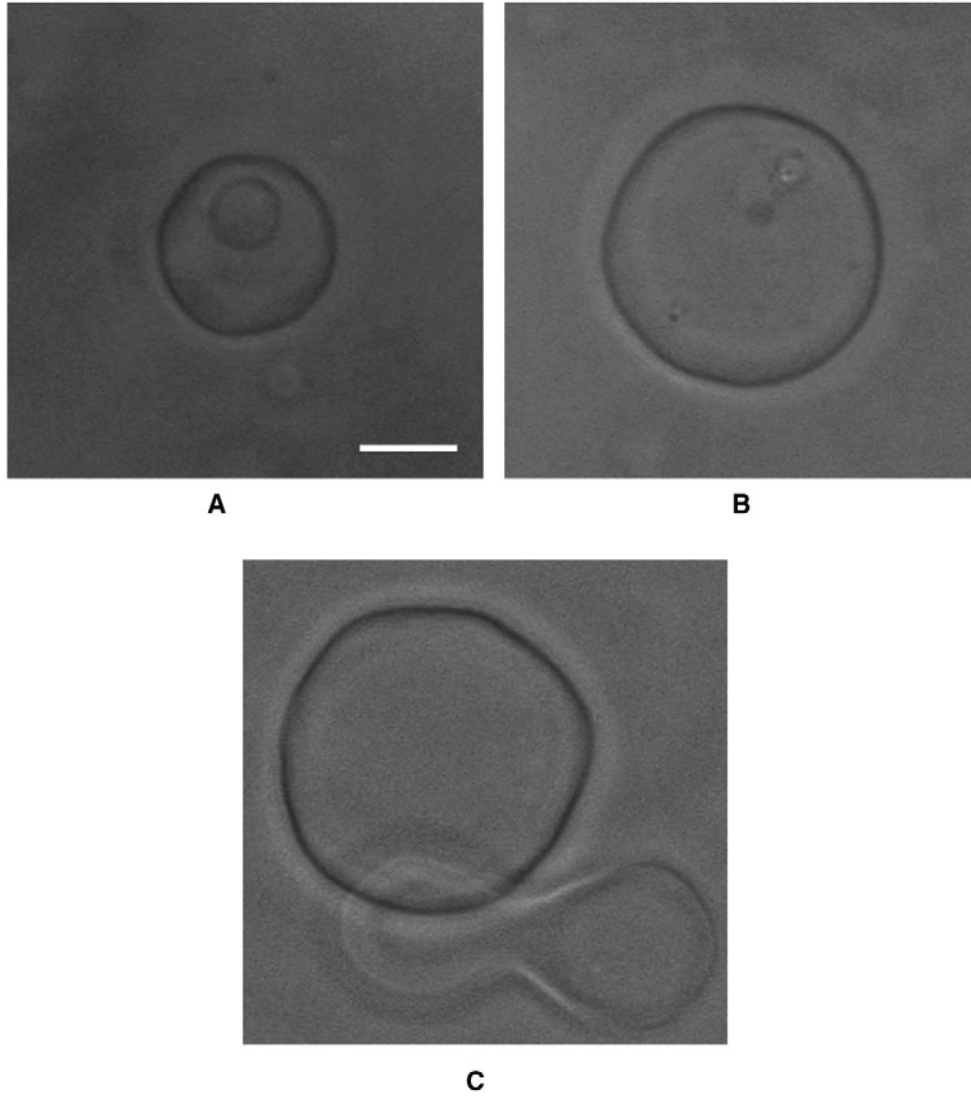


**Fig. 2.** Phase-contrast images of 3 typical DLPC giant vesicles in water. (A) GUV 1, a small flaccid vesicle with  $R = 8.7 \mu\text{m}$ , the vesicles inside and outside seeming unconnected. (B) GUV 2, a tense vesicle with  $R = 13.8 \mu\text{m}$ . (C) GUV 3, a flaccid vesicle with  $R = 15.8 \mu\text{m}$ , close to a bean-shaped vesicle below the focal plane apparently unconnected. The bar represents  $10 \mu\text{m}$ .

leading to the expression for the spherical harmonics  $Y_n^m(\theta, \varphi) = \mathcal{P}_n^m(\cos \theta) \cdot e^{im\varphi}$  [54] and

$$\begin{aligned} |U_n^0(t)|^2 &= |a_n^0(t)|^2, \\ |U_n^m(t)|^2 + |U_n^{-m}(t)|^2 &= \frac{1}{2} [|a_n^m(t)|^2 + |b_n^m(t)|^2], \\ &1 \leq m \leq n. \end{aligned} \quad (4)$$

The free energy  $F\{u_0, \delta u\}$  of a given shape defined by  $u_0 + \delta u$  with respect to that of the equilibrium one,  $F\{u_0\}$ , is simply [4, 55]

$$\begin{aligned} F\{u_0, \delta u\} - F\{u_0\} = \\ \frac{k_c}{2} \sum_{n=2}^{n_{\max}} \lambda_n(\bar{\sigma}) \left( |a_n^0(t)|^2 + \frac{1}{2} \sum_{1 \leq m \leq n} [|a_n^m(t)|^2 + |b_n^m(t)|^2] \right), \end{aligned} \quad (5)$$

where  $\lambda_n(\bar{\sigma}) = (n+2)(n-1)[\bar{\sigma} + n(n+1)]$  and  $\bar{\sigma}$  is the reduced membrane tension [4, 55]. Every  $a_n^m$  (or  $b_n^m$ ),  $1 \leq m \leq n$ , is an independent mode with a Boltzmann statistics proportional to  $\exp(-k_c \lambda_n(\bar{\sigma}) x^2 / 4k_B T)$  ( $x$  representing the possible  $a_n^m$  or  $b_n^m$  values) and a time average  $\langle |a_n^m(t)|^2 \rangle = 2k_B T / (k_c \lambda_n(\bar{\sigma}))$ .

Unfortunately, phase-contrast video-microscopy gives access to the contour only, *i.e.*, an equatorial cross-section defined by  $\theta = \pi/2$  (fig. 1). This contour is well defined (see bottom of fig. 1) and image analysis leads to a nice description of the contour fluctuations,  $r(\pi/2, \varphi, t) = \rho(\varphi, t)$ , as a function of the angle  $\varphi$ , and the time,  $t$ . Typically 300 points per contour are kept, corresponding to 300 discrete radii regularly distributed as a function of the  $\varphi$  directions (taking 600 or more contour points did not result in a better statistical description of GUV thermal fluctuations). Introducing  $\rho(t)$  as the angle average of the contour

for a given image recorded at time  $t$ , and  $R = \langle \rho(t) \rangle$  as the corresponding time average, we can write the relative contour fluctuations,  $v(\varphi, t) = (\rho(\varphi, t) - \rho(t))/R$ , as

$$v(\varphi, t) = \sum_{n=2}^{n_{\max}} \sum_{0 < |m| \leq n} U_n^m(t) \cdot Y_n^m\left(\frac{\pi}{2}, \varphi\right). \quad (6)$$

Equivalently,  $v(\varphi, t)$  can also be written using Fourier decomposition [28]. Rearranging, we find

$$v(\varphi, t) = \sum_{0 < m}^{n_{\max}} \left[ \cos(m\varphi) \sum_{n \geq m}^{n_{\max}} a_n^m(t) \cdot \mathcal{P}_n^m(0) + \sin(m\varphi) \sum_{n \geq m}^{n_{\max}} b_n^m(t) \cdot \mathcal{P}_n^m(0) \right] \quad (7)$$

and writing  $\alpha^m(t) = \sum_{n \geq m}^{n_{\max}} a_n^m(t) \cdot \mathcal{P}_n^m(0)$  and  $\beta^m(t) = \sum_{n \geq m}^{n_{\max}} b_n^m(t) \cdot \mathcal{P}_n^m(0)$ , we get

$$v(\varphi, t) = \sum_{0 < m}^{n_{\max}} \alpha^m(t) \cos(m\varphi) + \beta^m(t) \sin(m\varphi), \quad (8)$$

which describes the fluctuations of the contour that corresponds to GUV equatorial cross-section.

The Fourier decomposition of the contour fluctuations, eq. (8), is a linear combination of a large number of independent fluctuation modes with Boltzmann-type statistics. Consequently,  $\alpha^m(t)$  (respectively,  $\beta^m(t)$ ) above has also a Boltzmann-type statistics named  $A^m(y)$  (respectively,  $B^m(y)$ ), that can be expressed as

$$A^m(y) = B^m(y) \propto \exp\left(-\frac{y^2}{\sum_{n \geq m}^{n_{\max}} [\mathcal{P}_n^m(0)]^2 \sigma_n^2}\right), \quad (9)$$

with  $y = \alpha^m$  or  $\beta^m$  and

$$\begin{aligned} \sigma_n^2 &= \frac{4k_B T}{k_c(n+2)(n-1)[\bar{\sigma} + n(n+1)]} \\ &= \frac{4k_B T}{k_c} \times \frac{1}{\lambda_n(\bar{\sigma})}. \end{aligned} \quad (10)$$

Classically, we are using the autocorrelation function of the vesicle contour fluctuations,  $\xi(\gamma, t)$ , to access a measurement of the bending elasticity,  $k_c$ , and the reduced membrane tension,  $\bar{\sigma}$ , of a given giant vesicle [4]. Using the already introduced  $\alpha^m(t)$  and  $\beta^m(t)$ , we have [4, 55]

$$\begin{aligned} \xi(\gamma, t) &= \frac{1}{2\pi R^2} \int_{\varphi=0}^{2\pi} [\rho(\varphi + \gamma, t) - \rho(t)] \\ &\quad \times [\rho(\varphi, t) - \rho(t)] d\varphi = \sum_{0 < m}^{n_{\max}} \chi^m(t) \cos(m\gamma), \end{aligned} \quad (11)$$

with  $\chi^m(t) = ([\alpha^m(t)]^2 + [\beta^m(t)]^2)/2$ . Therefore, the autocorrelation function should be experimentally a sum of

positive terms when using Fourier decomposition. Moreover,  $\alpha^m(t)$  and  $\beta^m(t)$  having a Boltzmann statistics,  $\chi^m$ , should be characterized by a monoexponential distribution,  $\Gamma^m(\chi^m)$

$$\Gamma^m(\chi^m) \propto \exp\left[-R^m(k_c/k_B T, \bar{\sigma}) \frac{\chi^m}{2}\right], \quad (12)$$

with

$$R^m(k_c/k_B T, \bar{\sigma}) = \frac{k_c}{k_B T} \times \frac{1}{\sum_{n \geq m}^{n_{\max}} [\mathcal{P}_n^m(0)]^2 / \lambda_n(\bar{\sigma})}. \quad (13)$$

## 4 Results and discussion

The idea behind the statistical approach to contour fluctuation analysis was not only to gain precision in the determination of  $k_c$  but also to identify clear criteria of how perfectly, or imperfectly, a given GUV relates to the theory. To illustrate our approach, GUVs that possibly had some problems (attachments, ellipsoidal contour, etc.) were therefore recorded and analyzed intentionally. Figure 2 shows three typical freely moving DLPC GUVs as obtained by electroformation in water. It can easily be noticed that each of these three GUVs is in rather close contact with another vesicle. Unfortunately, from the images alone it is not possible to decide whether they are connected or not. Vesicle 1, shown in fig. 2A, is small, fluctuating and quasi-spherical. This GUV contains a smaller GUV in its inner volume that is apparently moving independently. Vesicle 2, fig. 2B, is much more tense and fluctuates poorly. During prolonged observation one can notice some small vesicles in its close vicinity, apparently freely moving without any direct contact to the GUV. Vesicle 3, fig. 2C, is rather flaccid but gives a strong contrast. The bean-shaped vesicle below the focal plane seems to be unconnected as far as can be judged from the images. Consequently, direct observations using optical video-microscopy indicated freely moving GUVs without obvious defects. Yet, all three GUVs are at risk of having a connection with another vesicle, which is a kind of defect that cannot be taken into account by the quasi-spherical vesicle model. These 3 vesicles were therefore good candidates to illustrate the advantages of the new method for  $k_c$  measurement.

### 4.1 Analysis of the fluctuation distributions

Due to the predicted monoexponential behavior of the  $\Gamma^m(\chi^m)$  distributions (obtained from cosine decomposition of the autocorrelation function of the contour fluctuation  $\xi(\gamma, t)$ ), the following presentation focuses on the study of the different  $\Gamma^m(\chi^m)$  as a function of  $m$  instead on either  $A^m(\alpha^m)$  or  $B^m(\beta^m)$ , the distributions of the contour fluctuations themselves. Fourier analysis of the autocorrelation function gives a series of  $\chi^m$  for every digitized contours, with typically  $2 \leq m \leq 30$ , eq. (11). For

a given mode  $m$ , we thus obtained  $N$  different  $\chi^m$  values as a function of the recorded time,  $t$ , some of them being very small in a range corresponding to frequent measurements, while others are very large and sparse. This frequency may be represented by simply using data binning (*i.e.*, a representation of the fraction of contours satisfying  $\chi_i - \Delta\chi/2 \leq \chi^m \leq \chi_i + \Delta\chi/2$  for increasing  $\chi_i$  ( $= i\Delta\chi$ ) of the experimentally determined  $\chi^m$  values). Likewise, one may use a direct frequency representation. Using an appropriate normalization factor, the  $N$  obtained  $\chi^m$  are sorted in increasing order, the smaller  $\chi_{\min}^m$  (close to 0) being most probable ( $\Gamma^m(\chi_{\min}^m) = 1$ ) and the larger  $\chi_{\max}^m$  being unlikely ( $\Gamma^m(\chi_{\max}^m) = 1/N$ ). Due to the very large number of contours analyzed per vesicle,  $N$ , we used this direct frequency representation. As will be shown in the following, such a representation allows easy identification of GUVs that deviate from the theoretically expected behavior.

Figure 3 depicts direct frequency representation of  $\chi^m/2$  for vesicles 1, 2 and 3 already shown in fig. 2. In the case of the small flaccid GUV 1, the distributions of the selected modes,  $\Gamma^m$ , as a function of the measured time-dependent amplitudes,  $\chi^m/2$ , follow nicely the expected monoexponential behavior (fig. 3A). However, one can notice some deviations from the monoexponential behavior for the 1% largest and uncommon amplitudes ( $\Gamma^m \leq 0.01$  corresponds typically to only  $\approx 150$  images). This can be attributed to the lack of statistics for these rare events. The  $\Gamma^m$  distributions of the tense GUV 2 also exhibit monoexponential behavior with the only exceptions being the occasional large amplitudes. However, one has to note that the range of the abscissa for the tense GUV 2 (fig. 3B) differs by a factor of about 4 when compared to the flaccid GUV 1 (fig. 3A). This is due to the strong reduction of the measurable fluctuations when working with a tense vesicle, that is characterized by a small excess area (large  $\bar{\sigma}$ ). Indeed a large  $\bar{\sigma}$ , eq. (10), is a damper for large thermal fluctuations typically up to  $n \sim 10$  [4] (more precisely, up to  $n \sim \sqrt{\bar{\sigma}}$ ). Finer analysis of the  $\Gamma^m$  distributions of vesicle 2 shows that  $\Gamma^2$  oscillates slightly but persistently around the expected monoexponential curve. Such a behavior is no longer detected for modes  $\geq 3$ , which are clearly monoexponential. The peculiar behavior of the 2nd mode can be understood considering typical relaxation times of thermal fluctuation as estimated by Milner & Safran's model [53]. For large GUVs, the second mode is characterized by relaxation times of about 30 s [56, 57]. In this case a recording of around 10 min is too short to gain a good statistical description of this second mode. Consequently, GUVs with a radius larger than  $10 \mu\text{m}$  often show non-ideal behavior for the 2nd mode, while showing the expected monoexponential decay for modes  $\geq 3$  (data not shown). In this case the 2nd mode should be reasonably rejected for  $k_c$  analysis, as every mode with poor statistical description.

Generally, monoexponential  $\Gamma^m$  distributions are indeed found for the vast majority of recorded GUVs which shows clearly that the thermal fluctuations of these GUVs can be adequately described by the theory. This is not the case for GUV 3. The  $\Gamma^m$  distributions for this vesicle differ significantly from the expected monoexponential behavior

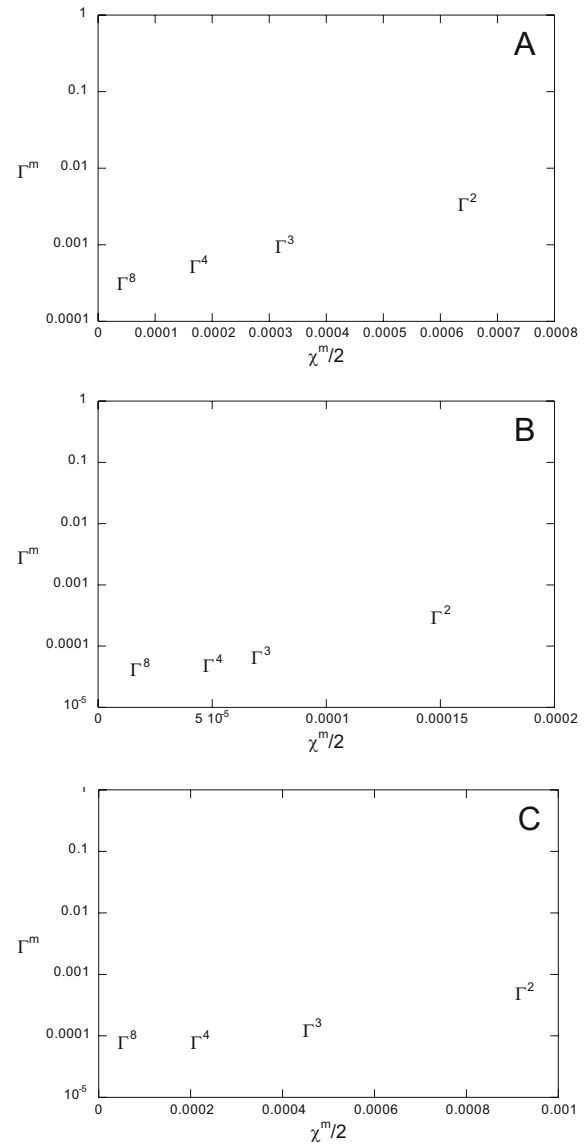


**Fig. 3.** Normalized distributions of the  $\chi^m/2$ ,  $2 \leq m \leq 8$  for the 3 typical DLPC vesicles previously shown in fig. 2. (A) Small flaccid GUV 1 with  $R = 8.7 \mu\text{m}$ . (B) Tense GUV 2 with  $R = 13.8 \mu\text{m}$ . (C) Flaccid GUV 3 with  $R = 15.8 \mu\text{m}$ .

whatever the frequency region (fig. 3C). Obviously GUV 3 has some kind of defect that results in thermal fluctuations that cannot be described by the quasi-spherical vesicle model. It might be speculated that GUV 3 is connected to the bean-shaped object below the focal plane (fig. 2C). In this case, its apparent membrane area (that corresponding to the quasi-spherical shape in the focus plane) would not be constant and could strongly fluctuate. These shape transformations are generally slow and do not occur often. Therefore, parts of the video could possibly correspond to apparent large excess areas (small  $\bar{\sigma}$ ) whereas others might be characterized by apparent smaller excess areas (high  $\bar{\sigma}$ ). Such different states of the membrane tension would give very different statistical distributions of the vesicle fluctuations that would be particularly visible for

smaller modes where the membrane tension is strongly influencing the mean fluctuation amplitude. However, even though we cannot be sure about the nature of the defect, the data clearly shows that this GUV should be excluded from analysis. In the following vesicle 3 will nevertheless be kept to show that our method retains this information about vesicle abnormality and that, more generally, our new method provides criteria for the objective rejections of GUVs without the need to examine individually the distributions of  $\Gamma^m$  as a function of the measured time-dependent amplitudes,  $\chi^m/2$ .

In order to determine bending elasticity from the experimental distributions of  $\chi^m/2$ , the decays observed in fig. 3 are fitted using a monoexponential. Obviously, this should be done by limiting the influence of outlier amplitudes. As already stated above, huge amplitudes are rare events with poor statistics. Therefore, they should be excluded from the fitting procedure. Amplitudes close to zero are the most frequent events but are also problematic. Contrariwise to huge amplitudes that can be measured precisely with an optical microscope, very small amplitudes are comparable to the resolution. Hence, they are noisy and should not be included in the fit. So the fitting procedure includes only amplitudes of a given order  $m$ ,  $\chi^m/2$ , that are in the “middle of the distribution”, *i.e.*,  $0.4 \geq \Gamma^m \geq 0.08$  (almost 30% of the digitized contours). The parameters obtained from the monoexponential fit are then used to determine the residuals over the full data range. A true monoexponential behavior will therefore lead to very small residuals on the whole data range while, on the contrary, an anomalous statistical distribution will show large residuals. This is illustrated in fig. 4 showing the 8th mode of the 3 different vesicles already discussed. For GUV 1 and 2, the fit of the middle of the distribution describes well the monoexponential behavior over the whole range of  $\Gamma^8$  (see fig. 4A where the open symbols correspond to the fitted middle of the distribution). In the case of GUV 3, the test function obtained from the fit describes well the distribution of the higher amplitudes, but diverges strongly for the small ones. Figure 4B shows the residuals obtained for the 8th mode of these three vesicles. To simplify the comparison between them, the abscissa was rescaled using  $R^8$ , eq. (13), obtained from the fitting procedure for the 3 GUVs. The window corresponding to  $0.4 \geq \Gamma^8 \geq 0.08$  is included in fig. 4 (vertical lines at  $R^8 \cdot \chi^8/2 = 0.92$  and  $2.52$ ). Vesicles 1 and 2 have very small residuals over the full range of amplitudes. It can therefore be concluded that the  $0.4 \geq \Gamma^8 \geq 0.08$  region ( $\approx 30\%$  of the images) predicts nicely the statistics of the full distribution. This is obviously not the case for vesicle 3. The corresponding residuals are minimized in the fitted region only, then strongly diverge for small amplitudes, *i.e.*, for  $0.4 < \Gamma^8$  ( $R^8 \cdot \chi^8/2 < 0.92$ ). This discrepancy between fitted curve and experimental data is used to rank the quality of the fitted exponentials, as a function of the order  $m$ . More precisely, the error estimation of the experimentally determined  $R^m$ , obtained from the exponential distribution of  $\chi^m$ , as a function of  $m$  is calculated from what it should be for the linearized distribution ( $\ln(\Gamma^m) = a - R^m \cdot \chi^m/2$ ,  $a$  being the logarithm

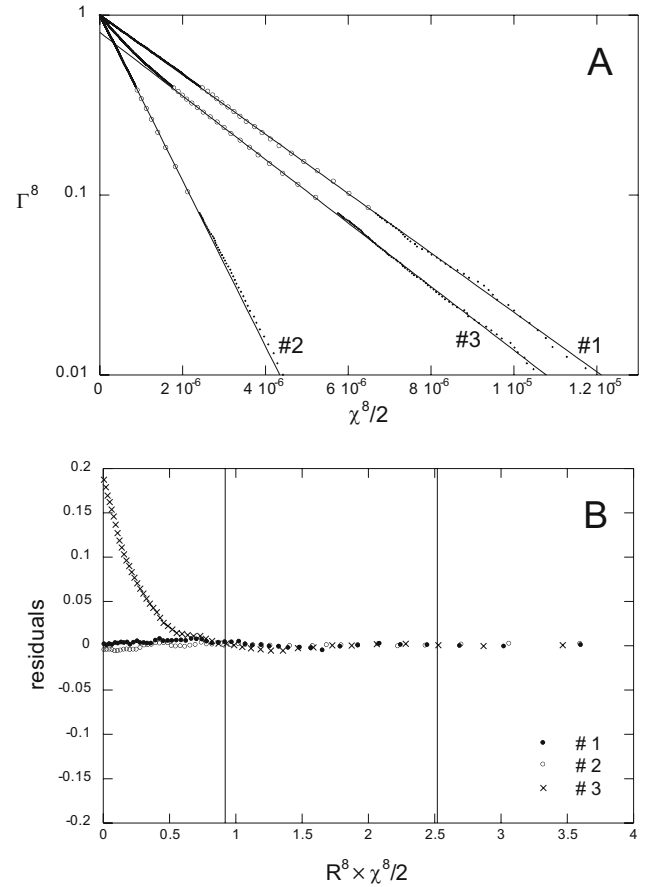


**Fig. 4.** (A) 8th-order distributions for the 3 DLPC GUVs presented in the previous figures. For clarity, the rare high-amplitude events are not represented. The continuous line corresponds to the exponential fit of the middle of the distribution, *i.e.*, the interval  $0.08 \leq \Gamma^8 \leq 0.4$  (open symbols). (B) Comparison of the residuals obtained for the 8th mode of these 3 GUVs over the whole data range in comparison with the exponential fit of the middle of the distribution (corresponding, after data rescaling, to the common window  $0.92 \leq R^8 \times \chi^8/2 \leq 2.52$ ).

of the exponential prefactor that should be close to 0 for normalized data) with the uncertainty,  $\sigma_{R^m}$ , associated with the slope  $R^m$  [58]

$$\sigma_{R^m} = \sqrt{\frac{N}{\sum_j (\chi_j/2)^2 - \left(\sum_j \chi_j/2\right)^2}} \simeq \frac{R^m}{\sqrt{N}},$$

the last term on the right being obtained in the case of an exponential distribution,  $j$  identifying the image index. To include the discrepancy between the obtained fitted parameters when considering  $0.4 \geq \Gamma^m \geq 0.08$  and the full data range, the above uncertainty,  $\sigma_{R^m}$ , is multiplied by a dimensionless number giving an estimation of the goodness of the fit. This number is directly the square root of the sum of the squares of the linearized distribution residuals,  $\sqrt{\sum_j (\ln[\Gamma^m(\chi_j^m/2)] - a + R^m \cdot \chi_j^m/2)^2}$ . Therefore,

the error  $\Delta R^m$  used in the following is eventually

$$\Delta R^m = \frac{R^m}{\sqrt{N}} \times \sqrt{\sum_i (\ln[\Gamma^m(\chi_i^m/2)] - a + R^m \cdot \chi_i^m/2)^2}.$$

This accounts explicitly for any deviation, huge or small, from the expected behavior. As can be seen in fig. 4B, the residuals of GUV 2 are slightly larger than those of GUV 1, a fact that will be preserved when determining bending elasticity for these vesicles.

## 4.2 Bending elasticity measurement of individual vesicles

The analysis of the amplitude statistics obtained from the Fourier decomposition of  $\xi(\gamma, t)$ , eq. (11), gave experimentally determined  $R_{\text{ex}}^m$  and  $\Delta R_{\text{ex}}^m$ , for typically  $2 \leq m \leq 30$ , used directly for the determination of bending elasticity. For a given vesicle, eq. (13) indicates that  $R_{\text{ex}}^m$  depends only on 2 parameters,  $k_c/k_B T$  and  $\bar{\sigma}$ , that can be obtained by a non-linear fitting procedure using a Levenberg-Marquardt method [58] that minimizes the merit function:

$$M(k_c/k_B T, \bar{\sigma}) = \sum_{m_{\min}}^{m_{\max}} \left[ \frac{R_{\text{ex}}^m - R_{\text{th}}^m}{\Delta R_{\text{ex}}^m} \right]^2.$$

In this expression,  $m_{\min}$  and  $m_{\max}$  are, respectively, the first and last relevant modes to consider in the analysis of the contour fluctuation statistics (see below) while  $R_{\text{th}}^m$  is the theoretical expression obtained in eq. (13). Note that in the denominator of the relation giving  $R_{\text{th}}^m$ , eq. (13), we also find a sum of a large number of positive terms depending on  $\bar{\sigma}$  only,  $\sum_{n \geq m} [\mathcal{P}_n^m(0)]^2 / \lambda_n(\bar{\sigma})$ , that slows down the fitting procedure leading to  $k_c/k_B T$  and  $\bar{\sigma}$ . Fortunately, the expression  $[\mathcal{P}_n^m(0)]^2 / \lambda_n(\bar{\sigma})$  is rapidly converging to zero when  $n$  increases compared to  $m$  for typical  $\bar{\sigma}$  values and the summation can be limited to the first few terms. In our case, we chose to sum from  $n = m$  to  $n = m + 10$ , knowing that  $\mathcal{P}_{m+2j+1}^m(0) = 0$  for  $j \geq 0$ .

At the end of this procedure, each vesicle is characterized by a particular bending elasticity at a given temperature,  $k_c$ , and a reduced membrane tension,  $\bar{\sigma}$ . These parameters are associated to error estimations for individual vesicle,  $\Delta k_c$  and  $\Delta \bar{\sigma}$ . From the covariance matrix, we also obtain the corresponding correlation coefficient,  $\text{Cor}(k_c, \bar{\sigma})$ , which testifies how strongly the estimates of  $k_c$  and  $\bar{\sigma}$  are coupled.

The result of this procedure is illustrated in fig. 5 using the data of GUV 1 and 3 to demonstrate the effect of measured thermal fluctuations that are either statistically correct, *i.e.*, GUV 1, or anomalous, *i.e.*, GUV 3. Figure 5A shows the  $R^m$  dependence as a function of  $m$  for vesicle 1. As already stated, this vesicle is characterized by individual  $R^m$  that are all associated with small error estimates,  $\Delta R^m$ , as reflected by the error bars. The first mode to consider in the minimization of the merit function  $M(k_c/k_B T, \bar{\sigma})$  for  $k_c/k_B T$  and  $\bar{\sigma}$  determination,

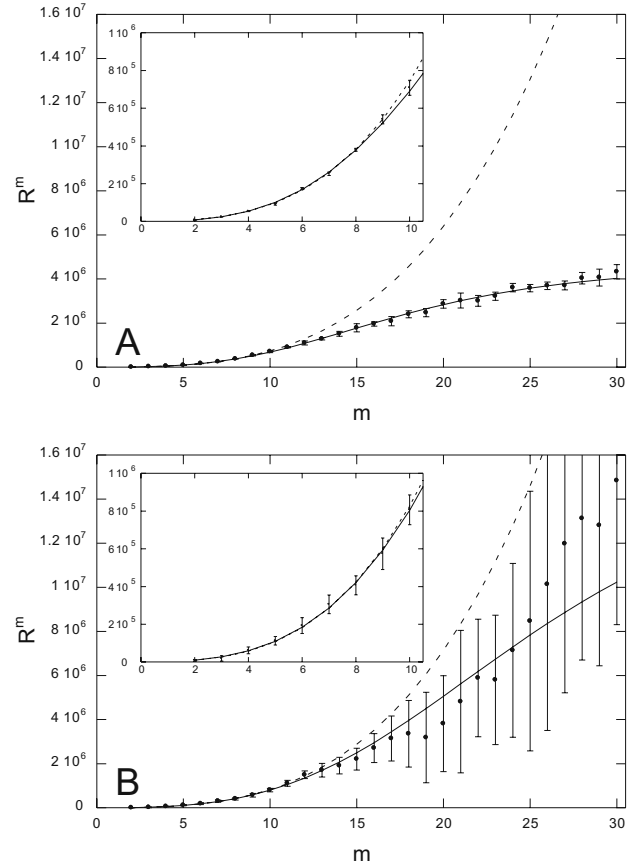


**Fig. 5.** (A)  $R^m$  values obtained from statistical analysis of the DLPC vesicle 1. The continuous line corresponds to a fit that includes the high  $m$  dependences ( $2 \leq m \leq 30$ ) by taking into account the contributing noise. One obtains  $k_c = (1.20 \pm 0.02) \times 10^{-19}$  J and  $\bar{\sigma} = 5.40 \pm 0.63$  ( $\text{Cor}(k_c, \bar{\sigma}) = -0.81$ ). The dashed line corresponds to a fit of  $2 \leq m \leq 10$  that does not account for the noise. (B) Same representation as in (A) for GUV 3 showing anomalous thermal fluctuations that translate into huge error bars for  $R^m$ .

$m_{\min}$ , that is the lowest mode with a good statistical description, is here  $m_{\min} = 2$ . The gradual increase of  $m_{\max}$  ( $m_{\max} > m_{\min}$ ) first improves the goodness of the fit [58] up to  $m_{\max} = 10$  (see the dashed line in fig. 5A and insert), then it worsens for higher  $m_{\max}$ . Taking into account the statistical probability  $Q$  that the obtained merit function  $M(k_c/k_B T, \bar{\sigma})$  should be exceeded by chance [58], we found in the case of vesicle 1,  $Q = 0.35$  for  $2 \leq m \leq 10$  with  $k_c = (1.09 \pm 0.02) \times 10^{-19}$  J.

In the case of GUV 2 (data not shown), the fitting procedure took into account the modes  $2 \leq m \leq 8$ , giving  $Q = 0.40$  and  $k_c = (3.21 \pm 0.43) \times 10^{-19}$  J, *i.e.*, a value for the bending elasticity much higher than for GUV 1. However, it should be noted that the situation is very different as well. The correlation coefficient between  $k_c$  and  $\bar{\sigma}$  for vesicle 2 is very close to  $-1$ . This means that the analysis of this tense vesicle yields a quite good estimation of the product  $k_c \times \bar{\sigma}$ , but not for the individual contributions of  $k_c$  or  $\bar{\sigma}$  (measurable fluctuation amplitude averages  $\langle |U_n^m(t)|^2 \rangle$ ) were mainly controlled

in such cases by the reduced membrane tension, *i.e.*,  $\langle U_n^m(t)^2 \rangle \approx k_B T / [k_c \bar{\sigma} (n+2)(n-1)]$  [4]). So  $k_c$  itself cannot be determined precisely. Consequently, the correlation coefficient is a first criterion for GUV exclusion for bending elasticity measurements. This criterion will objectively reject vesicles that are too tense for  $k_c$  measurement albeit they are nice objects for micromanipulation experiments [59] or optical observations using fluorescence microscopy [6]. From the numerous measurements done by our group, we conclude that GUVs with a correlation coefficient  $\leq -0.85$  are inappropriate for  $k_c$  measurements despite the fact that these GUVs may exhibit observable thermal fluctuations.

Taking now vesicle 3 as a counter example, we found  $m_{\min} = 2$  and an optimized goodness of the fit for  $m_{\max} = 12$  (dashed line in fig. 5B and insert). Contrary to vesicle 1, this large and flaccid vesicle 3 leads to  $Q = 1.00$  associated to a very small relative chi-squared value (“too good to be true” [58]) with  $k_c = (1.40 \pm 0.17) \times 10^{-19}$  J. Indeed, this  $Q$  value is easily explained by the very large error bars as estimated by the fitting procedure of the amplitude probabilities obtained from the Fourier analysis of  $\xi(\gamma, t)$ . Consequently the obtained  $k_c$  is associated to a large error estimate. As already stated earlier, this vesicle does not conform to the quasi-spherical model, probably because of a defect that could not be detected with the optical microscope, such as a large variation in the excess area that would be incompatible with the quasi-spherical model. Anyhow, from the analysis it becomes clear that there is no need to detect such a defect clearly. The “too good to be true” value of  $Q = 1.00$  reflects perfectly the poor quality of the individual  $R^m$  values and the underlying anomalous statistics and is as such a strong exclusion criterion.

More generally, we have to have a closer look on the choices made for the first and last modes  $m_{\min}$  and  $m_{\max}$  considered in the fitting procedure. While vesicles 1 to 3 gave positive estimated  $\bar{\sigma}$ , this is not always the case. In the case of negative  $\bar{\sigma}$  values corresponding to highly fluctuating vesicles, one cannot take into account the 2nd mode (and possibly the 3rd one) in the fitting procedure to increase the “goodness of the fit” that leads to bending elasticity and reduced membrane tension estimations. Also, depending on the vesicle, the fitting procedure can only be carried out on a given limited number of amplitudes (see fig. 5). Precisely, depending on  $\bar{\sigma}$  and the mean radius of the vesicle,  $m_{\max}$  could be found to be as large as 18 or as low as 5 or 6. Looking at higher modes (say,  $m > 20$ ), one clearly detects a saturation in the values of  $R^m$  associated with the increasing dominance of noise (see fig. 5A, the fitted dashed lines and the corresponding experimentally determined  $R^m$ ). This is a general feature revealed by the analysis. The measured  $R^m$  reached a limiting value roughly independent of the studied vesicle but dependent on the experimental set-up (objective magnification or video-camera) seemingly associated with noise. Intuitively one expects noise to come into play at some point, at least when coming close to the optical resolution.

At this point we have to come back to the experimentally determined  $A^m$  or  $B^m$  distributions introduced in the

theoretical section above. We observed Gaussian statistics whatever the value of  $m$ , with a width decreasing first with  $m$ , than becoming constant at high enough  $m$  values (data not shown). This is a white noise signature, the corresponding width  $\sigma_{\text{wn}}$  being defined by the set-up resolution and the electronic noise mainly associated with the video-camera. The measured  $\chi^m/2$  shown in fig. 3 being a sum of the squares of  $\alpha^m$  and  $\beta^m$ ,  $\chi^m/2 = [(\alpha^m)^2 + (\beta^m)^2]/4$ , high  $m$  values should correspond to exponential statistics characterized by  $R^m \sim 1/\sigma_{\text{wn}}^2$  while for smaller  $m$ ,  $R^m$  should be mainly controlled by thermal fluctuations as predicted by eq. (13).

In the intermediate  $m$  range, any measured  $R^m$  results from a superposition of thermal fluctuations,  $1/R_{\text{ff}}^m = k_B T / k_c (\sum_{n \geq m}^{n_{\max}} [\mathcal{P}_n^m(0)]^2 / \lambda_n(\bar{\sigma}))$  from eq. (13), and white noise,  $1/R_{\text{wn}}^m = \sigma_{\text{wn}}^2$ . Accordingly, the fitting procedure should include the contribution of white noise by a modification of eq. (13) with  $1/R^m = 1/R_{\text{ff}}^m + 1/R_{\text{wn}}^m$ :

$$R^m(k_c/k_B T, \bar{\sigma}, \sigma_{\text{wn}}) = \frac{1}{k_B T / k_c \left( \sum_{n \geq m}^{n_{\max}} [\mathcal{P}_n^m(0)]^2 / \lambda_n(\bar{\sigma}) \right) + \sigma_{\text{wn}}^2}. \quad (14)$$

This relation can be used directly to determine the bending elasticity  $k_c/k_B T$ , the reduced membrane tension,  $\bar{\sigma}$ , and the white noise parameter  $\sigma_{\text{wn}}$ . This 3-parameters-fitting procedure works generally very nicely as illustrated in fig. 5A (dashed line) using the data of vesicle 1. The number of modes maximizing  $Q$  up to 0.98 was this time much higher ( $2 \leq m \leq 30$ ) for a bending elasticity,  $k_c$ , equal to  $(1.20 \pm 0.02) \times 10^{-19}$  J and a reduced membrane tension,  $\bar{\sigma}$ , equal to  $5.40 \pm 0.63$ . We like to stress that using this fitting procedure a smaller  $m_{\max}$  (with also a smaller  $Q$ ) hardly affects the values obtained for  $k_c$  and  $\bar{\sigma}$ , as soon as  $m_{\max} \geq 16$ . Conversely, taking  $m_{\max} < 16$  leads to a badly defined white noise contribution associated to unpredictable modifications in the determined  $k_c$  and  $\bar{\sigma}$ . Amazingly, the noise contribution found for this vesicle corresponded approximately to the 40th mode amplitude, *i.e.*, a half-wavelength of about  $0.6 \mu\text{m}$  ( $= \pi R/m$ ), which is very close to the optical resolution of our microscope set-up. In the case of GUV 3 that does not obey to the quasi-spherical model, the inclusion of the white noise contribution in the fitting procedure does not change the situation. The fit is still characterized by  $Q = 1.00$ , *i.e.*, a “too good to be true” value as expected from the huge error bars for  $R^m$  for large  $m$ .

A recently published model introduced another term in the description of the spectrum of GUV thermal fluctuations [60,61], arising from hybrid modes that involve monolayer dilatational elasticity. Unfortunately, we were not able to detect the influence of this second term. This may be due to our experimental setup, which requires the choice of GUVs with a typical radius smaller than  $15 \mu\text{m}$  and  $m_{\max}$  usually smaller than 30 where white noise dominates the measured fluctuations.

In summary, this method works very well and gives stable and precise  $k_c$  values for GUVs that shows thermal fluctuation statistics that fit the theoretical model. For

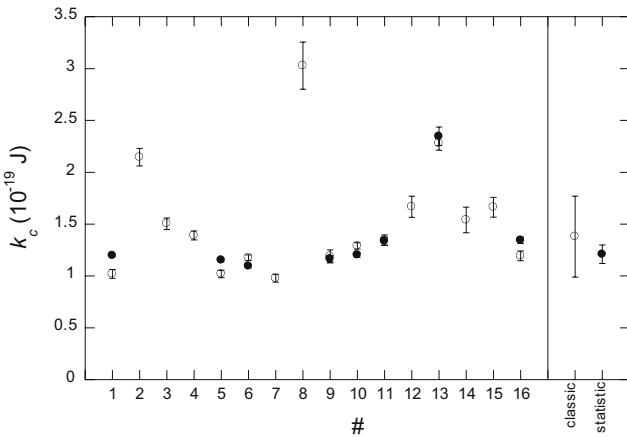


**Fig. 6.** Left side: individual bending elasticities of 16 different DLPC GUVs in deionized water that were recorded and analyzed without any prior selection based on size, membrane tension or possible connection. The classical method ( $\circ$ ) results in highly dispersed bending elasticity values while the statistical method ( $\bullet$ ) rejects about half the vesicles. Right side: bending elasticity averages when using the classical method ( $\circ$ ) or the statistical approach ( $\bullet$ ). The bilamellar vesicle 13 was not taken into account (see text for details).

vesicles that do not match this model, the method yields strong and objective rejection criteria. As a simple “rule of thumb” for a given number of individual  $k_c$  values, we generally need to analyze twice, or thrice, the number of vesicles. Albeit this may be considered as somewhat arduous, this method has the clear advantage of not only determining bending elasticity with a very high accuracy but also of obtaining  $k_c$  of individual GUVs that are extremely close to the mean  $k_c$  value as we will show in the following.

### 4.3 Comparison of the statistically based method for bending elasticity measurements with the classical approach

Figure 6 shows the bending elasticities obtained by the classical approach and the new statistical method for 16 different DLPC GUVs in water where vesicles 1, 2 and 3 correspond to those we already discussed earlier in the text. We like to stress that all vesicles were recorded as soon as they were found in the observation chamber, without any consideration of their “quality”. Precisely, we kept indifferently small, huge, highly or poorly fluctuating GUVs. Obviously, this is not the usual procedure. Generally a selection on medium size GUVs (radius from 7 to 15  $\mu\text{m}$ ) with a reasonable membrane tension ( $\bar{\sigma} \approx 0$ ) and no apparent contact with neighboring vesicles is made prior to recording. The seemingly hazardous approach to liposome recording employed herein is used to test the robustness of the statistically based method to distinguish between GUVs that are coherent with the theoretical description of thermal fluctuations of quasi-spherical vesicles and those that are not.

As can be seen in fig. 6 (open dots), the individual bending elasticity measurements of DLPC GUVs using the classical method based on the Legendre polynomials decomposition of  $\xi(\gamma, t)$  [4] yield very scattered  $k_c$  values comprised between  $0.98 \times 10^{-19}$  J and  $3.21 \times 10^{-19}$  J. Naturally, this results in a badly defined mean value of  $k_{c,\text{DLPC}}^{\text{classic}} = (1.38 \pm 0.39) \times 10^{-19}$  J. With  $k_c$  that poorly defined, it would of course be impossible to detect any subtle effect on bending elasticity caused by the addition of a membrane inclusion or aqueous solutes [62]. Examination of the  $k_c$  data obtained by the statistical method to the very same vesicle set (fig. 6, black dots) reveals the rejection of half of all recorded GUVs. Only 8 vesicles were kept, the other ones being eliminated based on objective criteria, *i.e.*, statistics incompatible with the quasi-spherical vesicle theory, overall poor statistics (low number of intact vesicle contours or high noise level) or strong correlation between  $k_c$  and  $\bar{\sigma}$  ( $\text{Cor}(k_c, \bar{\sigma}) \approx -1$ ). In other words, the statistical method suppresses  $k_c$  values of GUVs with hidden defects, GUVs with recordings of poor quality and GUVs that are too tense. It should be emphasized that recordings of poor quality are quite frequent. For instance, for large and floppy vesicles, it is generally extremely difficult to maintain the whole contour line in the focal plane of the optical microscope. This leads to a large number of incomplete contours that are rejected during the analysis and ends up with a poor statistical description of the GUVs thermal fluctuations. Similarly, very small vesicles ( $R \leq 7 \mu\text{m}$ ) lead to poor statistics albeit not for the same reasons. Small GUVs are easy to record and yield large numbers of complete contours. Nevertheless, their small size and their associated small amplitude thermal fluctuations translate into high noise levels, justifying their exclusion in the statistical-based treatment.

We will now focus on some individual vesicles, especially the three GUVs already discussed in the previous section. Vesicle 1 gave very small error estimates both for bending elasticity and reduced membrane tension when including a large mode number ( $2 \leq m \leq 30$ ,  $k_c^{\text{stat}} = (1.20 \pm 0.02) \times 10^{-19}$  J). Actually, this value is a bit higher but better defined than what can be obtained with the classical method of bending elasticity measurement based on Legendre polynomials decomposition of the autocorrelation function [4, 55], *i.e.*  $k_c^{\text{classic}} = (1.02 \pm 0.04) \times 10^{-19}$  J. The difference between the two values arises from the number of modes included into the analysis. In the case of the classical method, the noise contribution cannot be taken into account which limits the analysis to the 10th mode. Consequently, the statistical method extracts more information from this GUV than the classical one. Also, in the classical analysis,  $k_c$  is obtained by fitting the mean  $B_n$  with their associated errors simply defined as the standard error. This standard error for a given  $B_n$  does not include any information about the actual quality of the statistics with respect to the theory. The statistical method solves this intrinsic problem. One can notice for example in fig. 5A that the amplitude probabilities obtained from the Fourier analysis,  $R^m$ , are less well defined for  $m = 15$  and 20 than those of the modes close to them, meaning that their influence in the fitting procedure will

be reduced. Therefore, we conclude that the new statistical method leads to a much better description of individual  $k_c$  measurements with an associated error that includes significant information about the quality of the GUV. This point can also be nicely demonstrated using GUV 2 and 3. The statistical analysis rejects them both, GUV 2 due to  $\text{Cor}(k_c, \bar{\sigma}) \approx -1$  and GUV 3 due to statistics incompatible with the theory. Using the classical method, they gave  $k_c^{\text{classic}} = (2.15 \pm 0.02) \times 10^{-19}$  J and  $k_c^{\text{classic}} = (1.50 \pm 0.01) \times 10^{-19}$  J, respectively. It may be noticed that both error bars are unrealistic small and do not reflect the quality of the data. This is especially obvious for vesicle 3 that did not fluctuate like a quasi-spherical GUV, probably due to a connection with the flaccid bean-shaped vesicle seen in fig. 2C. In the classical analysis this important information does simply not show up and GUVs like this are retained and finally add up to the uncertainty of the mean  $k_c$  value of a system.

From fig. 6 it can also be seen that the classical method leads to three  $k_c$  values that are higher than  $2 \times 10^{-19}$  J (GUV 2, 8 and 13) and clearly not in accordance with published values [29, 63]. A typical approach in such cases is to exclude them using the argument that the corresponding vesicles should be bi- or multi-lamellar, yet typically without any real proof of this multilamellarity. In the statistical method, vesicles 2 and 8 are excluded due to objective criteria not related to multilamellarity. GUV 13 had good statistics with thermal fluctuations obeying the quasi-spherical vesicle theory. Its individual bending elasticity was found to be equal to  $k_c^{\text{stat}} = (2.35 \pm 0.09) \times 10^{-19}$  J and is the only outlier found by the statistical method. All other vesicles retained in the statistical method gave very similar results with  $k_c$  values around  $1.2 \times 10^{-19}$  J. It is usually assumed that the effective bending elasticity of a bilamellar quasi-spherical GUV is twice that of a unilamellar one [64, 65], just what we found for this vesicle. If GUV 13 is truly bilamellar this should also be observable from the images. Precisely, under identical optical parameters the intensity variation across the membrane position for a bilamellar GUV should be characterized either by a higher contrast (*i.e.*, a higher peak with respect to background), or by a larger width compared to a unilamellar GUV. Figure 7 compares the intensity variation from 2 video images of vesicle 13 ( $R = 7.93 \mu\text{m}$ ) with that of vesicle 9 characterized by a similar radius ( $R = 7.68 \mu\text{m}$ ) after background subtraction. The intensity (vertical axis) is dependent on the pixel position (horizontal axis) when crossing the vesicle membrane, the peaks localizing the membrane position. Indeed, the intensity of the peaks of these 2 GUVs are similar but the contour thickness of GUV 13 is found to be significantly larger than that of GUV 9, which confirms the idea of a bilamellar vesicle. Excluding this bilamellar vesicle in the statistical analysis gives  $k_{c,\text{DLPC}}^{\text{stat}} = (1.21 \pm 0.09) \times 10^{-19}$  J as the average bending elasticity of the system. This is somewhat higher than the  $0.92 \times 10^{-19}$  J found about 15 years ago [29]. There are several reasons for this discrepancy. The number of images at the time was very low (less than 500) compared to nowadays (about 15000), the resolution was also smaller and there was a correction factor accounting

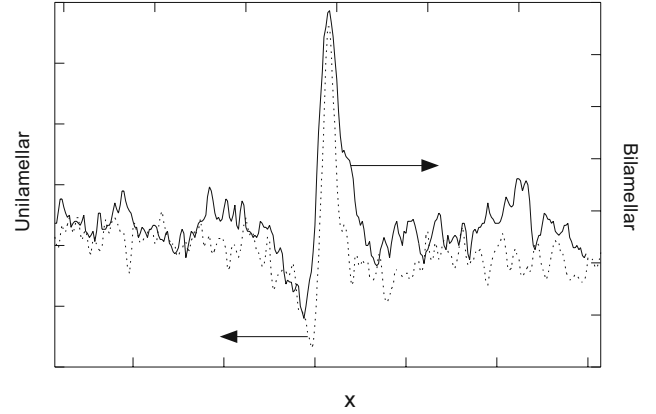


**Fig. 7.** Comparison of the intensity profile (vertical axis where high intensity corresponds to membrane localization) as a function of the pixel position (horizontal axis) on a horizontal line crossing the membrane contour for 2 vesicles with comparable radii. The dashed line corresponds to a unilamellar GUV with a bending elasticity close to the average (GUV 9), the continuous line to GUV 13 with a bending elasticity about twice the average.

for the video integration time [4, 31] that is not needed for the instantaneous-like images obtained by the stroboscopic illumination. Also, the ITO-electrodes used 15 years ago have since long been replaced by Pt-electrodes as ITO electrodes were shown to increase the peroxidation rate of unsaturated lipids [66].

We can now summarize the different GUV selection criteria discussed before. The first criterion to consider is the vesicle size. Small vesicles ( $R < 10 \times R_{\text{opt}}$ , where  $R_{\text{opt}}$  is the optical resolution) should not be considered to maintain a good precision in the membrane position and large vesicle should not be recorded because their deformations are too slow to relax. In the case of our set-up, we limit the analysis to GUVs with a radius from 7 to 20  $\mu\text{m}$ . The second criterion is related to the statistical dependence of the bending elasticity modulus and reduced membrane tension. This dependence is estimated by the correlation coefficient  $\text{Cor}(k_c, \bar{\sigma})$ . We found that reliable bending elasticity measurements are obtained when the results are characterized by  $\text{Cor}(k_c, \bar{\sigma}) \geq -0.85$ . The last criterion concerns the quality of the fitting procedure as measured by the  $Q$  factor. We considered the data from a given GUV to be considered when  $Q \geq 0.2$ . Care must be taken when  $Q$  approaches 1. If such value is due to badly defined mode analysis due to poor statistics like GUV 3, the obtained bending elasticity modulus should not be considered any longer. These 2 last criteria are strongly dependent on the chosen  $m_{\text{min}}$  and  $m_{\text{max}}$  that should be optimized to improve the value of either  $\text{Cor}(k_c, \bar{\sigma})$  or  $Q$ .

Finally, it is worthwhile to comment on the dispersions of the individual bending elasticity values for this batch of not so carefully selected GUVs. Using the classical method the dispersion is extremely large. Eliminating manually the so-called outliers (GUV 2, 8 and 13) reduces significantly the dispersion to  $k_{c,\text{DLPC}}^{\text{classic}} = (1.27 \pm 0.17) \times 10^{-19}$  J. Although this kind of manual selection is not unusual, it

is scientifically not satisfying because of the absence of any explanation why these outliers occur. The statistical method gives  $k_{c,DLPC}^{\text{stat}} = (1.21 \pm 0.09) \times 10^{-19}$  J meaning that the dispersion is about the half of the latter. Besides the already mentioned help for an unbiased choice of the well-behaved vesicles, this is another essential advantage of our new approach. We definitively obtained a smaller dispersion of the bending elasticity measurements from one vesicle to the other (improved reproducibility) that could help the observation of tiny dependences of bending elasticity with physical or chemical factors (temperature effects [29,63], membrane additives [14,18,49]).

#### 4.4 Bending elasticity of POPC bilayers containing different fluorescent dyes

As already mentioned, this new statistical analysis reinforces the confidence in the determination of bending elasticity of individual GUVs, making possible the tracking of changes in the bending elasticity between individual GUVs in the same electroformation cell. One may imagine such changes resulting from differences in composition that arise during electroformation or other processes that affect the GUVs after formation. For example, photo-induced phenomena, such as lipid peroxidation, will necessarily individualize GUVs observed by video-microscopy as they depend on the intensity and duration of the light exposure of each individual GUV. Indeed, focusing on the influence of fluorescent dyes on the bending elasticity of POPC GUVs and using this new statistical method, we were able to highlight photo-induced lipid peroxidation triggered by some membrane fluorescent dyes [38]. These results are briefly presented in the following to illustrate the advantage of the statistical method to detect inhomogeneous systems (for details on the study, see [38]).

Six different fluorescent dyes were chosen according to their frequent usage as membrane probes (see for instance [6] and references therein), namely Rh-DPPE, DiIC18, TR-DPPE, Bodipy-PC, NBD-PC and LAURDAN. POPC containing 2 mol% of one of these dyes was used to produce GUVs in buffer (1 mmol/L Tris and 1 mmol/L EDTA adjusted to pH 7.4). In the absence of fluorescent dyes, we obtained a mean bending elasticity value of  $k_{c,POPC}^{\text{stat}} = (1.29 \pm 0.04) \times 10^{-19}$  J for POPC bilayers in low concentration Tris/EDTA buffer. As for DLPC in water, the dispersion of individual  $k_c$  values is much smaller using the statistical method than the classical one. Again, this shows the improved reproducibility in bending elasticity measurements from one vesicle to the other. Using the statistical method, small dispersions in individual  $k_c$  values were also found in the case of POPC GUVs containing 2 mol% LAURDAN, DiIC18 or TR-DPPE. For these admittedly high dye concentrations, LAURDAN and DiIC18 induced only very slight changes in overall bending elasticity, whereas TR-DPPE leads to a small but significant reduction in  $k_c$ . A very different behavior was observed for GUVs containing 2 mol% Rh-DPPE, NBD-PC or Bodipy-PC. For the latter, the dispersions in  $k_c$  values were found to be anomalously

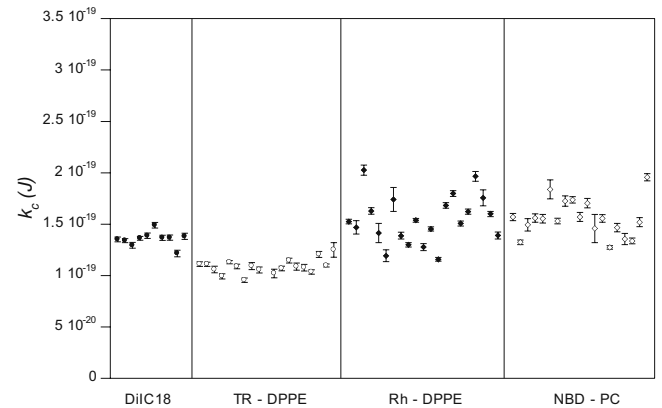


**Fig. 8.** Comparison of the individual bending elasticities obtained with POPC GUVs containing 2 mol% of DiIC18 (●), TR-DPPE (○), Rh-DPPE (◆) or NBD-PC (◇) fluorescent dyes.

large despite the use of the statistical method. Figure 8 shows the individual  $k_c$  values obtained in the case of DiIC18, TR-DPPE, Rh-DPPE and NBD-PC, while those with LAURDAN and Bodipy-PC are not displayed to ease up the presentation. As can be seen, the reproducibility in bending elasticity measurements is good for DiIC18 and TR-DPPE containing GUVs. Individual  $k_c$  values fluctuate around a well-defined mean value as can be expected for a homogeneous system. This is not the case for Rh-DPPE and NBD-PC containing GUVs. Individual  $k_c$  values are extremely scattered. A verification of the vesicle quality kept by the analysis confirmed that they all had good statistics, fluctuated according to the quasi-spherical vesicle theory and fulfilled all selection criteria. Also, error bars of individual GUVs are overall very small for these systems, showing that  $k_c$  determination is accurate. So, for Rh-DPPE, NBD-PC and Bodipy-PC (data not shown) containing GUVs, this lack of reproducibility has to be based on a true individualization of the GUV behavior. This has been attributed to dye-triggered light-induced peroxide formation, leading to GUVs with varying peroxide content depending on the illumination power and exposure length they received individually [38].

In fact, light-induced domain formation has already been reported in GUVs containing several lipids [66–69]. With respect to the new method, we like to stress that this detection of variations in peroxide content in vesicle bilayers might have been minimized or masked with the classical method based only on the averages of the fluctuation amplitudes [4], due to its inherently low reliability in the measurement of individual  $k_c$  values (see also fig. 6) and its absence of objective selection criteria. In the context of membrane anchored fluorescent dyes, the new statistical method for the measurement of bending elasticity has shown its usefulness. By use of this technique we detected lipid-peroxide formation at levels too low to result in macroscopic domain formation, that would actually prohibit  $k_c$  measurements. This highlights the sensibility of bending elasticity to small changes in lipid composition and underlines the need for high-precision measurement of  $k_c$ .

## 5 Conclusion

In this work, we showed that the statistical analysis of giant unilamellar vesicle thermal fluctuations results in a large improvement of the reproducibility in the bending elasticity measurement. This new method is based on the intrinsic Gaussian distributions of the thermal fluctuations, understood using the well-known quasi-spherical model still valid since its first application in this context [4, 53]. The statistical analysis allows proper selection, based on unbiased criteria, of GUV for which the quasi-spherical model applies objectively. Also, the new method accounts explicitly for the uncertainty in the statistics of each mode used to determine bending elasticity as well as the contribution of white noise. Together, these improvements yield average bending elasticities of unprecedented high precision as well as a confident measurement of  $k_c$  from individual GUVs. This is crucial to detect small changes in the bending elasticity caused, for instance, by environment alterations such as temperature, pH or solute concentration or by changes in the bilayer composition. A further advantage is that the statistical method can also be used when a GUV system becomes inhomogeneous, a situation that may arise due to a chemical reaction or some slow molecular rearrangement that affect individual GUVs differently. This was demonstrated herein by the example of photo-induced lipid peroxidation triggered by some fluorescent dyes and may be useful in the context of lipid raft, domain formation or other complex phenomenon.

This work was made possible due to a collaboration between MEMPHYS - Center for Membrane Biophysics, supported by the Danish National Research Foundation (Grundforskningsfonden), and the UMR-CNRS 6226, supported by the Centre National de la Recherche Scientifique (CNRS).

## References

- G. Beblík, R.M. Servuss, W. Helfrich, *J. Phys. (Paris)* **46**, 1773 (1985).
- H. Engelhardt, H.P. Duwe, E. Sackmann, *J. Phys. (Paris) Lett.* **46**, L395 (1985).
- E. Evans, D. Needham, *J. Phys. Chem.* **91**, 4219 (1987).
- J.F. Faucon *et al.*, *J. Phys. (Paris)* **50**, 2389 (1989).
- E. Evans, W. Rawicz, *Phys. Rev. Lett.* **64**, 2094 (1990).
- L.A. Bagatolli, *BBA - Biomembranes* **1758**, 1541 (2006).
- L.A. Bagatolli, E. Gratton, *Biophys. J.* **78**, 290 (2000).
- L.A. Bagatolli, E. Gratton, *Biophys. J.* **77**, 2090 (1999).
- J. Korlach *et al.*, *Proc. Natl. Acad. Sci. U.S.A.* **96**, 8461 (1999).
- L.R. Montes *et al.*, *Biophys. J.* **93**, 3548 (2007).
- J. Bernardino de la Serna *et al.*, *J. Biol. Chem.* **279**, 40715 (2004).
- C. Dietrich *et al.*, *Biophys. J.* **80**, 1417 (2001).
- I. Plasencia, L. Norlén, L.A. Bagatolli, *Biophys. J.* **93**, 3142 (2007).
- P. Méléard *et al.*, *Biophys. J.* **72**, 2616 (1997).
- S.L. Veatch, S.L. Keller, *BBA - Mol. Cell Res.* **1746**, 172 (2005).
- T. Pott, H. Bouvrais, P. Méléard, *Chem. Phys. Lipids* **154**, 115 (2008).
- P. Méléard, L.A. Bagatolli, T. Pott, in *Methods in Enzymology*, edited by N. Düzgüneş, Vol. **465** (Academic Press, Burlington, 2009) p. 161.
- H. Bouvrais *et al.*, *Biophys. Chem.* **137**, 7 (2008).
- P. Walde *et al.*, *ChemBioChem* **11**, 848 (2010).
- T. Shimanouchi, H. Umakoshi, R. Kuboi, *Langmuir* **25**, 4835 (2009).
- T.J. Politano *et al.*, *Colloid Surf. B* **79**, 75 (2010).
- K.S. Horger *et al.*, *J. Am. Chem. Soc.* **131**, 1810 (2009).
- W. Helfrich, *Z. Naturforsch.* **28c**, 693 (1973).
- F. Brochard, J.-F. Lennon, *J. Phys. (Paris)* **36**, 1035 (1975).
- M.B. Schneider, J.T. Jenkins, W.W. Webb, *Biophys. J.* **45**, 891 (1984).
- R.M. Servuss, W. Harbich, W. Helfrich, *BBA - Biomembranes* **436**, 900 (1976).
- I. Bivas *et al.*, *J. Phys. (Paris)* **48**, 855 (1987).
- H.P. Duwe, J. Käs, E. Sackmann, *J. Phys. (Paris)* **51**, 945 (1990).
- L. Fernandez-Puente *et al.*, *Europhys. Lett.* **28**, 181 (1994).
- J. Henriksen, A.C. Rowat, J.H. Ipsen, *Eur. Biophys. J.* **33**, 732 (2004).
- P. Méléard *et al.*, *Europhys. Lett.* **19**, 267 (1992).
- P. Méléard *et al.*, *Biochimie* **80**, 401 (1998).
- J. Pécréaux *et al.*, *Eur. Phys. J. E* **13**, 277 (2004).
- E. Sackmann, H.P. Duwe, H. Engelhardt, *Faraday Discuss. Chem. Soc.* **81**, 7132 (1986).
- M.B. Schneider, J.T. Jenkins, W.W. Webb, *J. Phys. (Paris)* **45**, 1457 (1984).
- E. Evans, *Biophys. J.* **43**, 27 (1983).
- J.R. Henriksen, J.H. Ipsen, *Eur. Phys. J. E* **14**, 149 (2004).
- W. Rawicz *et al.*, *Biophys. J.* **79**, 328 (2000).
- L. Bo, R.E. Waugh, *Biophys. J.* **55**, 509 (1989).
- J. Song, R.E. Waugh, *Biophys. J.* **64**, 1967 (1993).
- R.E. Waugh, R.M. Hochmuth, *Biophys. J.* **52**, 391 (1987).
- R. Dimova, B. Pouligny, C. Dietrich, *Biophys. J.* **79**, 340 (2000).
- C.H. Lee, W.C. Lin, J. Wang, *Phys. Rev. E* **64**, 20901 (2001).
- C.H. Lee, W.C. Lin, J. Wang, *2000 Conference on Lasers and Electro-Optics (Nice, 2000)*, p. 592.
- C.H. Lee, W.C. Lin, J. Wang, *Opt. Commun.* **135**, 233 (1997).
- M. Kummrow, W. Helfrich, *Phys. Rev. A* **44**, 8356 (1991).
- Y. Lyatskaya *et al.*, *Phys. Rev. E* **63**, 11907 (2000).
- J.P. Reeves, R.M. Dowben, *J. Cell Physiol.* **73**, 49 (1969).
- H. Bouvrais *et al.*, *BBA - Biomembranes* **1798**, 1333 (2010).
- P. Méléard *et al.*, *Europhys. Lett.* **19**, 267 (1992).
- J. Genova *et al.*, *J. Optoelectron. Adv. Mater.* **31**, 68 (2005).
- J. Genova *et al.*, *Bulg. J. Phys.* **31**, 68 (2004).
- S.T. Milner, S.A. Safran, *Phys. Rev. A* **36**, 4371 (1987).
- G. Arfken, *Mathematical Methods for Physicists*, 3rd edition (Academic Press, Inc. Boston, 1985).
- M.D. Mitov *et al.*, *Advances in Supramolecular Chemistry*, edited by G.W. Gokel, Vol. **II** (Jai Press, Inc., Greenwich, 1992) p. 93.
- P. Méléard *et al.*, *Europhys. Lett.* **11**, 355 (1990).
- T. Pott, P. Méléard, *Europhys. Lett.* **59**, 87 (2002).

58. W.H. Press *et al.*, *Numerical Recipes in C. The Art of Scientific Computing*, 2nd edition (Cambridge University Press, New York, 1992).
59. W. Rawicz *et al.*, *Biophys. J.* **94**, 4725 (2008).
60. R. Rodriguez-Garcia *et al.*, *Phys. Rev. Lett.* **102**, 128101 (2009).
61. L.R. Arriaga *et al.*, *Eur. Phys. J. E* **31**, 105 (2010).
62. H. Bouvrais *et al.*, *Biophys. J.* **96**, 161a (2009).
63. T. Honger *et al.*, *Phys. Rev. Lett.* **72**, 3911 (1994).
64. D. Marsh, *Chem. Phys. Lipids* **144**, 146 (2006).
65. A.G. Petrov, I. Bivas, *Prog. Surf. Sci.* **16**, 389 (1984).
66. A.G. Ayuyan, F.S. Cohen, *Biophys. J.* **91**, 2172 (2006).
67. G.W. Feigenson, *BBA - Biomembranes* **1788**, 47 (2009).
68. J. Yuan *et al.*, *J. Am. Chem. Soc.* **130**, 2067 (2008).
69. J. Zhao *et al.*, *BBA - Biomembranes* **1768**, 2777 (2007).